SUPPLEMENTARY INFORMATION

Structural basis for cell surface patterning through NetrinG-NGL interactions

Elena Seiradake, Charlotte H. Coles, Pavel Perestenko, Karl Harlos, Jeff McIlhinney, A. Radu Aricescu & E. Yvonne Jones

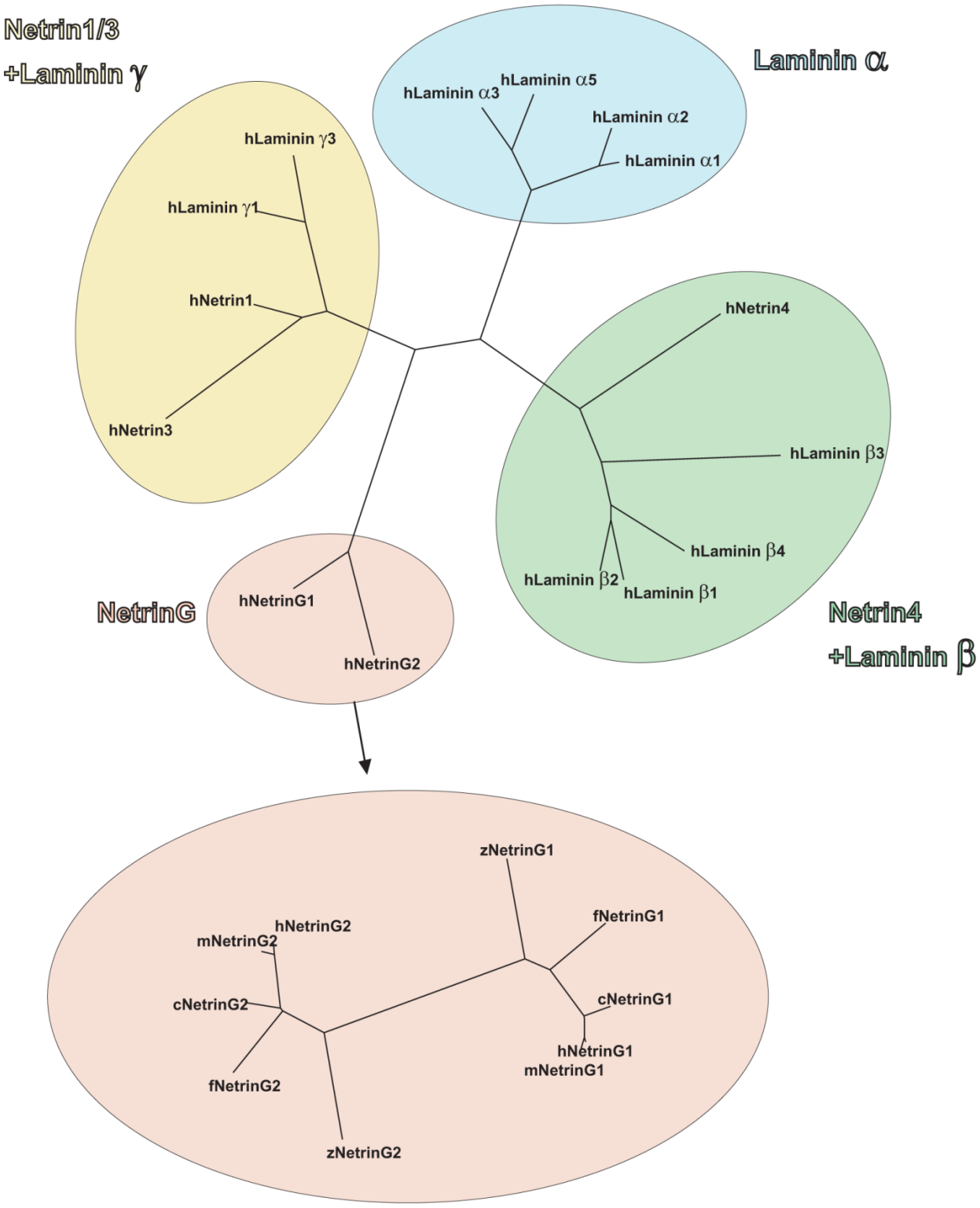

Supplementary figure 1. Family tree of Netrin and Laminin N-terminal Lam domains. Branch distances are based on sequence alignment and were calculated with programs from the PHYLIP package (Felsenstein, 1993). h=human, m=mouse, c= chicken, f= frog, z= zebrafish. The N-terminal domain of Netrin5 differs from the Lam consensus sequence and was not included in the analysis.

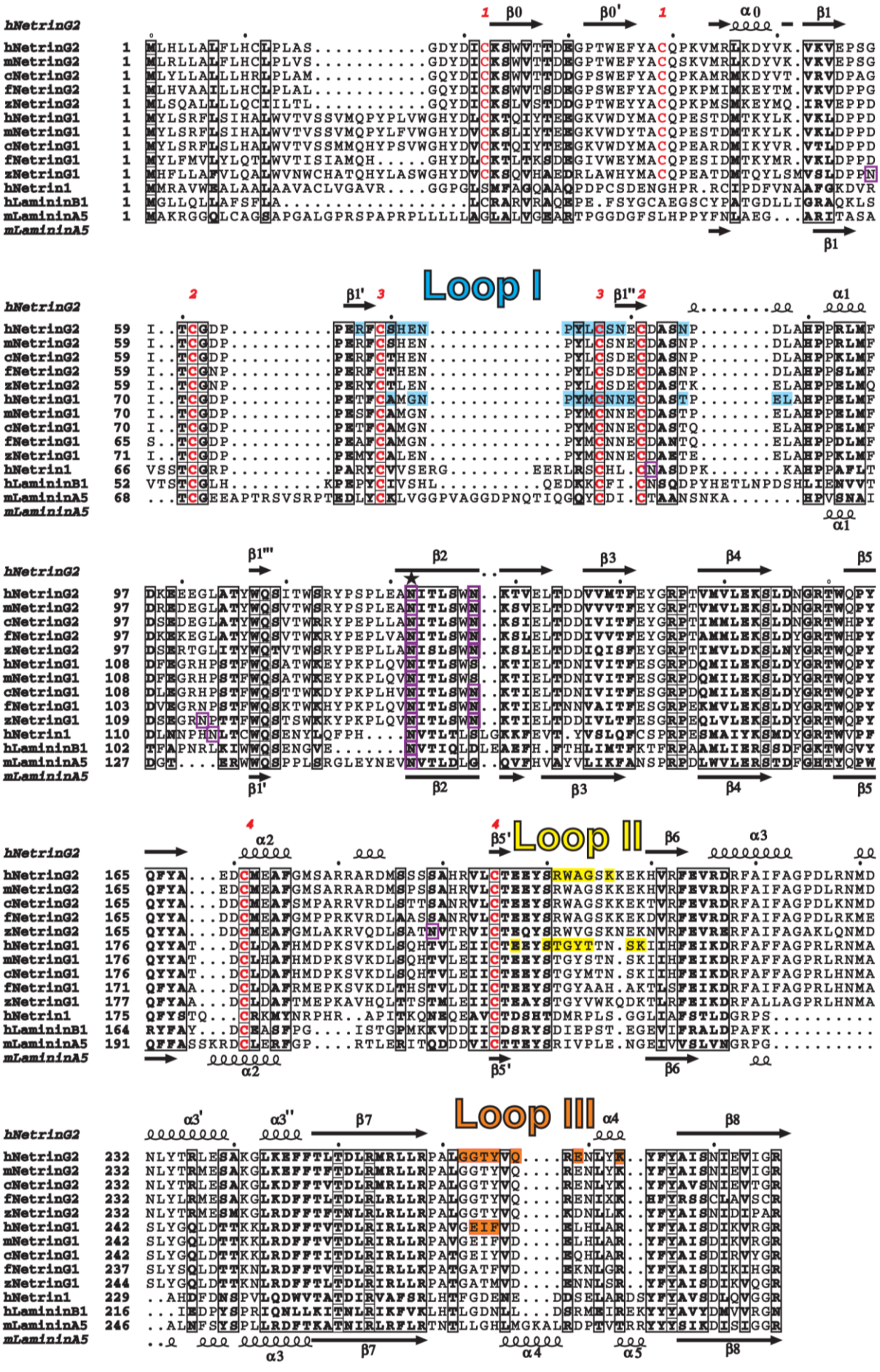
Loop I
Loop II
Loop III

Supplementary figure 2. Sequence alignment of NetrinG and laminin N-terminal Lam domains. Secondary structure elements found in the human NetrinG2 and mouse LamininA5 (Hussain et al, 2011) structures are indicated above and below the alignment, respectively. Cysteine pairs forming disulfide bridges in human NetrinG2 are colored red and paired by numbers above the alignment. A predicted N-linked glycosylation site, which was visible in the NetrinG and LamininA5 structures, is marked with a black star. Asparagine residues (N) predicted to carry glycans are outlined with a purple box (Gupta et al, 2004, in preparation). Residues contacting NGL in the complex crystal structures are highlighted by a coloured background box: blue for loop I, yellow for loop II and orange for loop III. h=human, m=mouse, c= chicken, f= frog, z= zebrafish.

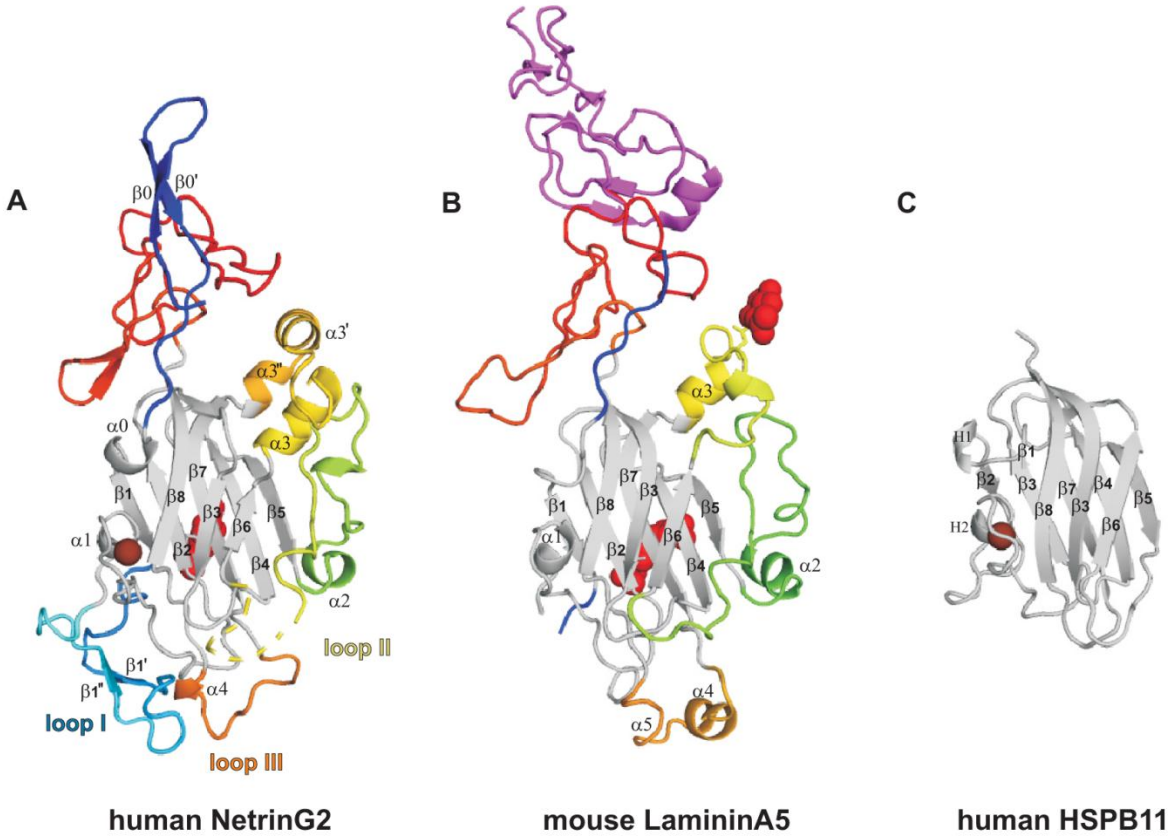

Supplementary figure 3. The N-terminal lam-domains of NetrinG2, Laminin A5 and HSPB11 share a similar beta-sandwich core (Ramelot et al, 2009). N-linked sugars are shown as red spheres and include a glycan on β2, predicted to be conserved among netrins and laminins. A structural calcium ion conserved in HSPB11 and NetrinG2 is depicted in brown. (A) Ribbon diagram of unliganded human NetrinG2$_{\text{Lam-EGF1}}$. Loop II is disordered in apo NetrinG2. Its position when NetrinG2 is in complex with NGL2 is indicated with a dotted yellow line. (B) Ribbon diagram of mouse Laminin A5 (Hussain et al, 2011). (C) Ribbon diagram of human HSPB11 (Ramelot et al, 2009).

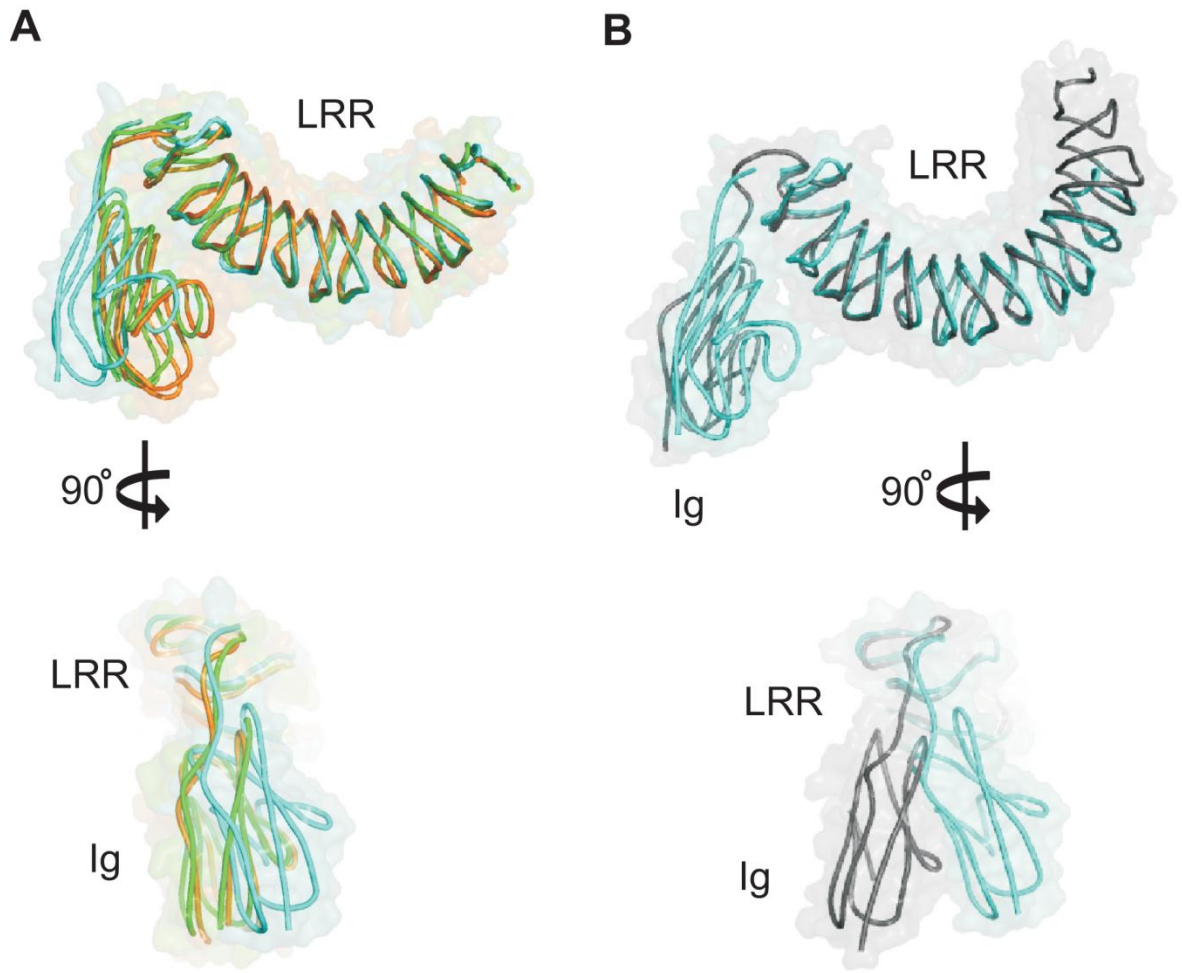

Supplementary figure 4. Variation in the relative orientations of the NGL and Lingo1 LRR and Ig domains. (A) $NGL1_{LRR\text{-}Ig}$ (cyan), $NGL2_{LRR\text{-}Ig}$ (green) and $NGL3_{LRR\text{-}Ig}$ (orange) were superposed via the LRR domains. (B) $NGL1_{LRR\text{-}Ig}$ (cyan) and $Lingo1_{LRR\text{-}Ig}$ (grey, (Mosyak et al, 2006)) were superposed via the LRR domains.

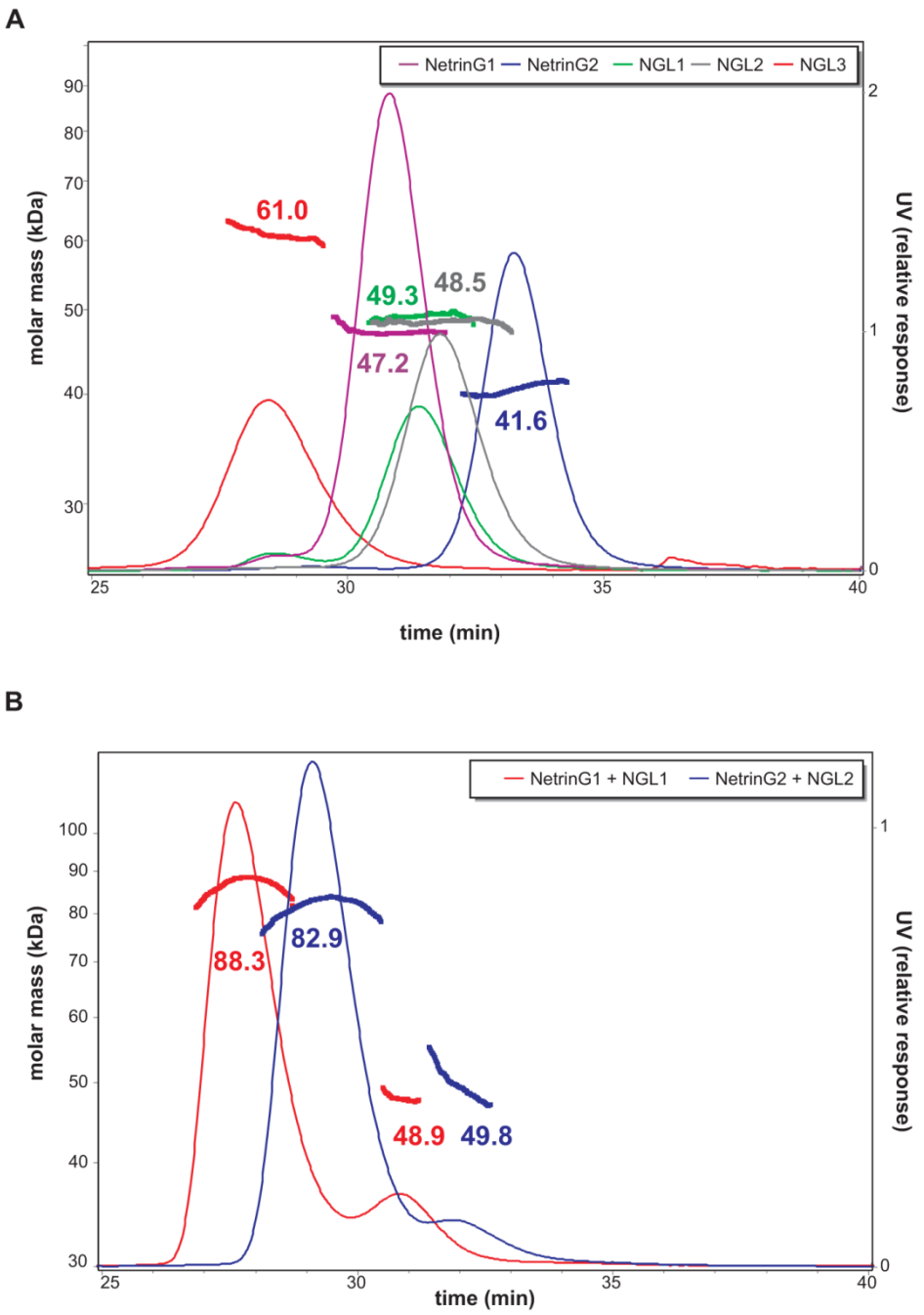

Supplementary figure 5. Multiple angle light scattering results suggest NetrinG$_{Lam\text{-}EGF}$ and NGL$_{LRR\text{-}Ig}$ are monomers in solution and form 1:1 complexes. (A) UV traces (relative response units) and molar masses (kDa) are shown as thin and thick lines, respectively, for unliganded NetrinG$_{Lam\text{-}EGF}$ and NGL$_{LRR\text{-}Ig}$. The purified proteins contain glycans added by HEK293T cells (for NGL3$_{LRR\text{-}Ig}$) or GnTI-deficient HEK293S cells (Aricescu et al, 2006; Chang et al, 2007) (for NetrinG1/2 $_{Lam\text{-}EGF}$, NGL1/2$_{LRR\text{-}Ig}$). The measured masses are in general agreement with masses predicted based on the primary sequence plus 1.34 kDa mass per potential N-linked glycosylation site for protein produced in GnTI-deficient HEK293S cells, or 2.06 kDa per site for protein produced in HEK293T cells. Thus the predicted molecular masses for fully glycosylated proteins (protein mass + glycan mass) are NetrinG1$_{Lam\text{-}EGF}$= 46.3+2.7 kDa, NetrinG2$_{Lam\text{-}EGF}$= 37.8+4.0 kDa, NGL1$_{LRR\text{-}Ig}$= 49.3+8.0 kDa, NGL2$_{LRR\text{-}Ig}$= 48.7+6.7 kDa, NGL3$_{LRR\text{-}Ig}$=42.2+16.5 kDa. (B) UV traces and molar masses (in kDa) are shown for NetrinG$_{Lam\text{-}EGF}$ - NGL$_{LRR\text{-}Ig}$ complexes.

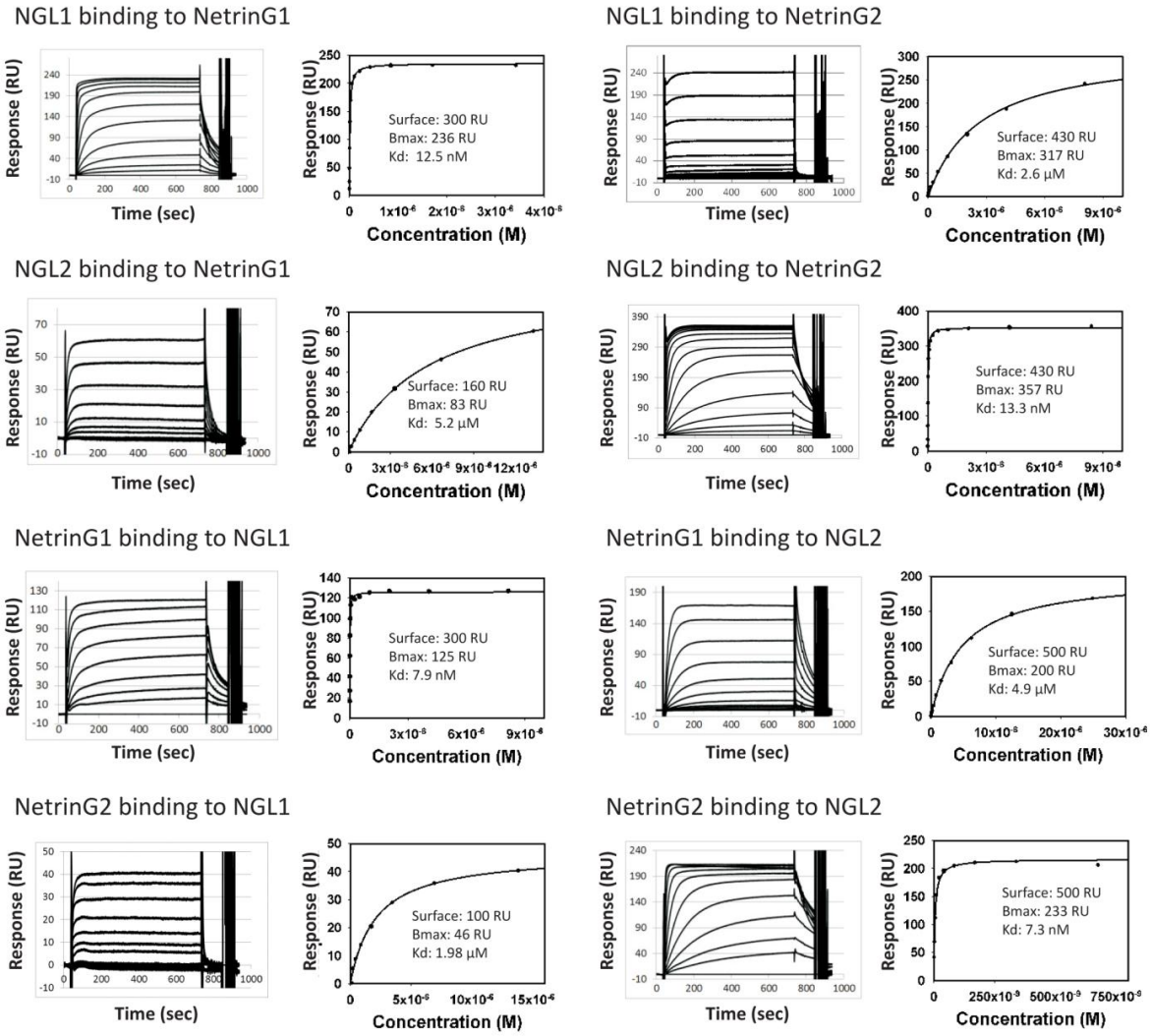

Supplementary figure 6. NGL-NetrinG intra-class binding is >100 times stronger than cross-class binding. Sensograms and fitted data (1:1 Langmuir binding model) are presented for binding of wild type $NGL1_{LRR\text{-}Ig}$ and $NGL2_{LRR\text{-}Ig}$ to $NetrinG1_{Lam\text{-}EGF1/4}$ and $NetrinG2_{Lam\text{-}EGF1}$ constructs. Using a shorter version of NetrinG1, which lacks EGF4 and therefore is equivalent to $NetrinG2_{Lam\text{-}EGF1}$ in its domain composition, resulted in the same NGL1- and NGL2 binding affinities as measured for $NetrinG1_{Lam\text{-}EGF1/4}$, demonstrating that EGF4 does not affect binding (unpublished observation). Depending on the experimental set-up, previous measurements of NetrinG-NGL affinities had shown some variation in the calculated K_d values. In a solid-phase binding assay (Lin et al, 2003), performed prior to the discovery of the NetrinG2-NGL2 interaction, binding of soluble NGL1 to microtitre wells coated with NetrinG1 was measured as giving a K_d= 1.6 nM. Similarly, in an ELISA assay using immobilized NetrinG2, an affinity of 2.5 nM was reported for the NetrinG2-NGL2 interaction (Zhang et al, 2008) and no affinity was detected between immobilized NetrinG1 and NGL2. In an SPR assay, where the ligands were directly immobilized on the sensor chip, the affinity measured for the NetrinG1-NGL1 interaction was K_d= 155 nM, and K_d= 377 nM for the NetrinG2-NGL2 interaction (Nishimura-Akiyoshi et al, 2007). Again, cross-class interactions were not detected, presumably in this case due to the overall lower level of binding measured in the alternative experimental conditions chosen (Nishimura-Akiyoshi et al, 2007).

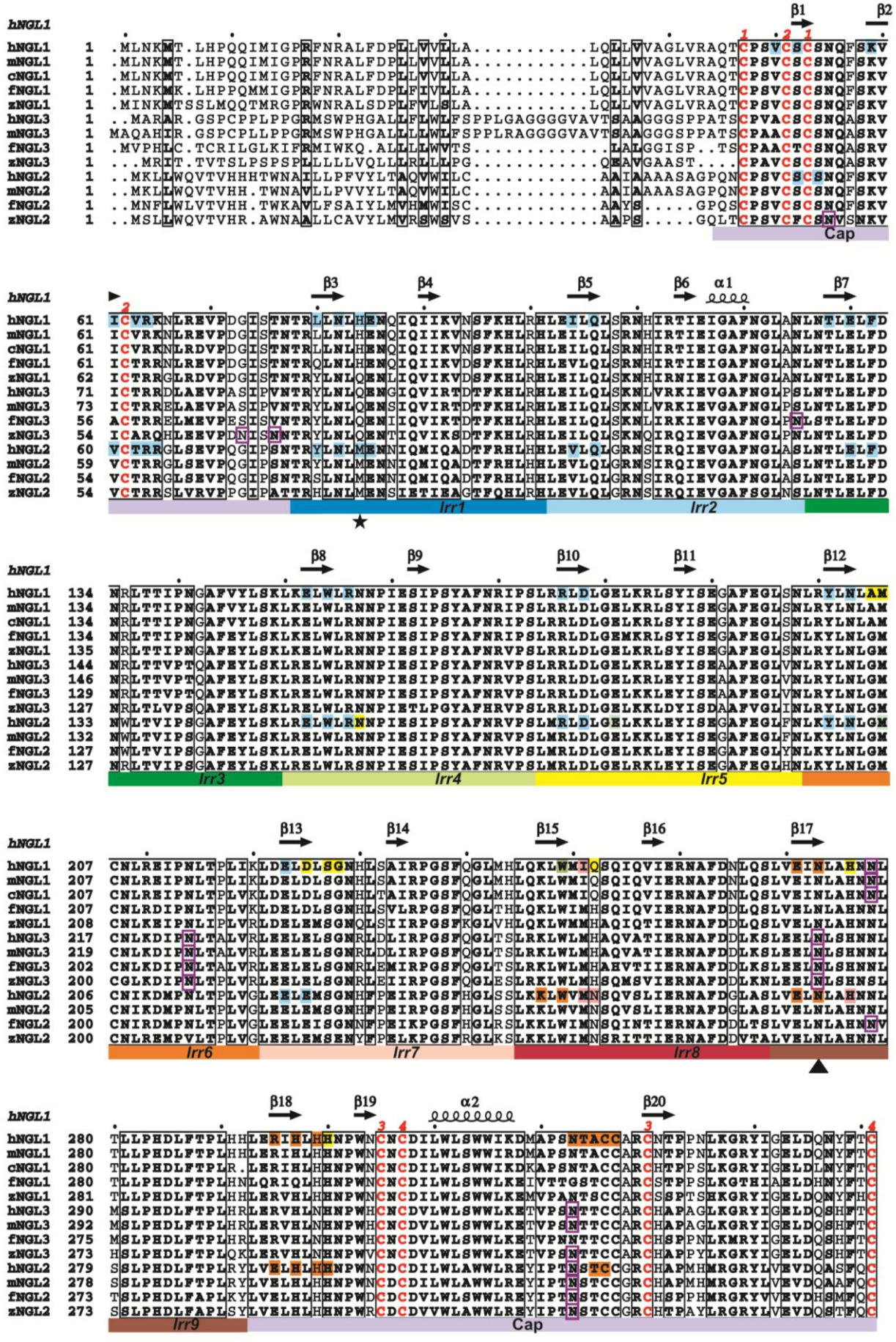
hNGL1
β1
β2
Cap
β3
β4
β5
β6
α1
β7
lrr1
lrr2
β8
β9
β10
β11
β12
lrr3
lrr4
lrr5
β13
β14
β15
β16
β17
lrr6
lrr7
lrr8
β18
β19
α2
β20
lrr9
Cap

Supplementary figure 7. Sequence alignment of NGL LRR domains. Secondary structure elements found in human NGL1 are indicated above the alignment, cysteine pairs forming disulfide bridges are in red and numbered above the alignment. Asparagine residues (N) predicted to carry glycans are highlighted with purple boxes (Gupta et al, 2004, in preparation). A black star indicates the position of NGL3 Q96, a residue important in the interaction with its cognate receptor, the RPTP LAR (Kwon et al, 2010); a black triangle marks a predicted N-linked glycosylation site in the concave face of NGL3 LRR. Residues contacting NetrinG loops I-III in the complex crystal structures are highlighted by a coloured background box: blue for loop I, yellow for loop II, orange for loop III, aquamarine for loops I+II, green for loops I+III, pink for loops II+III. h=human, m=mouse, c= chicken, f= frog, z= zebrafish.

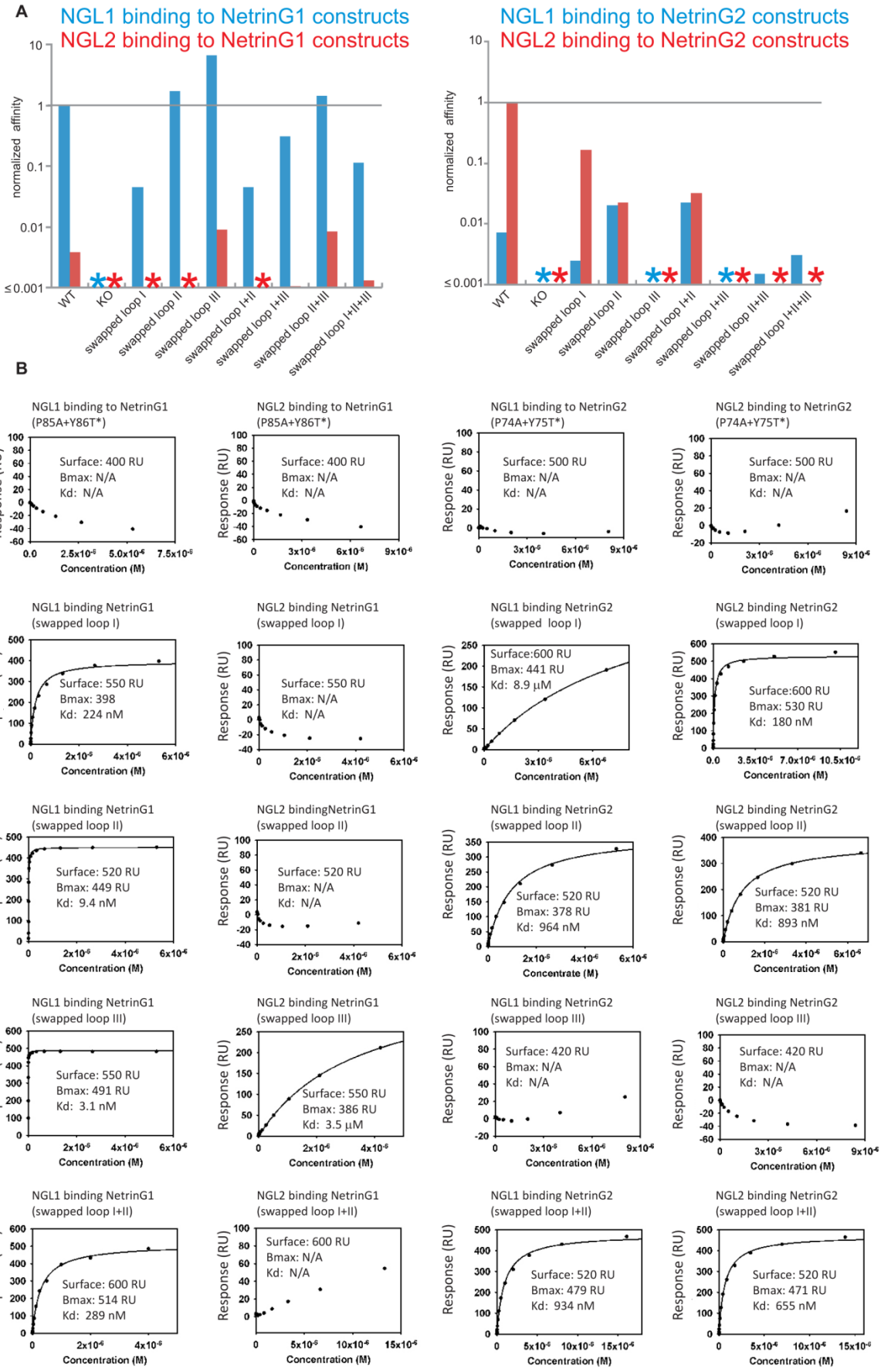
A
NGL1 binding to NetrinG1 constructs
NGL2 binding to NetrinG1 constructs
normalized affinity
10
1
0.1
0.01
≤ 0.001
WT
KO
swapped loop I
swapped loop II
swapped loop III
swapped loop I+II
swapped loop I+III
swapped loop II+III
swapped loop I+II+III
NGL1 binding to NetrinG2 constructs
NGL2 binding to NetrinG2 constructs
B
NGL1 binding to NetrinG1 (P85A+Y86T*)
Surface: 400 RU
Bmax: N/A
Kd: N/A
NGL2 binding to NetrinG1 (P85A+Y86T*)
Surface: 400 RU
Bmax: N/A
Kd: N/A
NGL1 binding to NetrinG2 (P74A+Y75T*)
Surface: 500 RU
Bmax: N/A
Kd: N/A
NGL2 binding to NetrinG2 (P74A+Y75T*)
Surface: 500 RU
Bmax: N/A
Kd: N/A
NGL1 binding NetrinG1 (swapped loop I)
Surface: 550 RU
Bmax: 398
Kd: 224 nM
NGL2 binding NetrinG1 (swapped loop I)
Surface: 550 RU
Bmax: N/A
Kd: N/A
NGL1 binding NetrinG2 (swapped loop I)
Surface:600 RU
Bmax: 441 RU
Kd: 8.9 µM
NGL2 binding NetrinG2 (swapped loop I)
Surface:600 RU
Bmax: 530 RU
Kd: 180 nM
NGL1 binding NetrinG1 (swapped loop II)
Surface: 520 RU
Bmax: 449 RU
Kd: 9.4 nM
NGL2 bindingNetrinG1 (swapped loop II)
Surface: 520 RU
Bmax: N/A
Kd: N/A
NGL1 binding NetrinG2 (swapped loop II)
Surface: 520 RU
Bmax: 378 RU
Kd: 964 nM
NGL2 binding NetrinG2 (swapped loop II)
Surface: 520 RU
Bmax: 381 RU
Kd: 893 nM
NGL1 binding NetrinG1 (swapped loop III)
Surface: 550 RU
Bmax: 491 RU
Kd: 3.1 nM
NGL2 binding NetrinG1 (swapped loop III)
Surface: 550 RU
Bmax: 386 RU
Kd: 3.5 µM
NGL1 binding NetrinG2 (swapped loop III)
Surface: 420 RU
Bmax: N/A
Kd: N/A
NGL2 binding NetrinG2 (swapped loop III)
Surface: 420 RU
Bmax: N/A
Kd: N/A
NGL1 binding NetrinG1 (swapped loop I+II)
Surface: 600 RU
Bmax: 514 RU
Kd: 289 nM
NGL2 binding NetrinG1 (swapped loop I+II)
Surface: 600 RU
Bmax: N/A
Kd: N/A
NGL1 binding NetrinG2 (swapped loop I+II)
Surface: 520 RU
Bmax: 479 RU
Kd: 934 nM
NGL2 binding NetrinG2 (swapped loop I+II)
Surface: 520 RU
Bmax: 471 RU
Kd: 655 nM
Response (RU)
Concentration (M)
Concentrate (M)

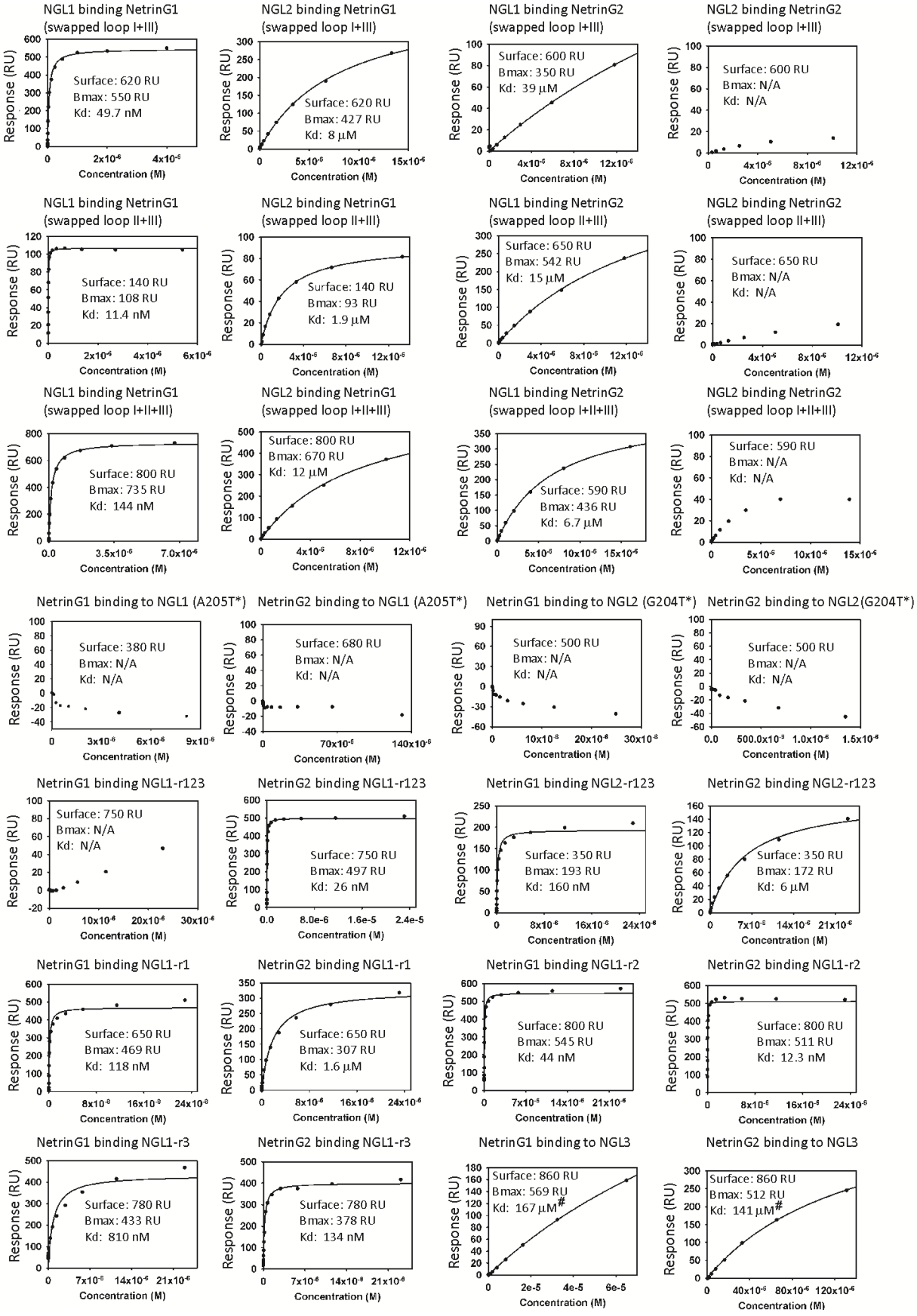
NGL1 binding NetrinG1 (swapped loop I+III)
Surface: 620 RU
Bmax: 550 RU
Kd: 49.7 nM
NGL2 binding NetrinG1 (swapped loop I+III)
Surface: 620 RU
Bmax: 427 RU
Kd: 8 µM
NGL1 binding NetrinG2 (swapped loop I+III)
Surface: 600 RU
Bmax: 350 RU
Kd: 39 µM
NGL2 binding NetrinG2 (swapped loop I+III)
Surface: 600 RU
Bmax: N/A
Kd: N/A
NGL1 binding NetrinG1 (swapped loop II+III)
Surface: 140 RU
Bmax: 108 RU
Kd: 11.4 nM
NGL2 binding NetrinG1 (swapped loop II+III)
Surface: 140 RU
Bmax: 93 RU
Kd: 1.9 µM
NGL1 binding NetrinG2 (swapped loop II+III)
Surface: 650 RU
Bmax: 542 RU
Kd: 15 µM
NGL2 binding NetrinG2 (swapped loop II+III)
Surface: 650 RU
Bmax: N/A
Kd: N/A
NGL1 binding NetrinG1 (swapped loop I+II+III)
Surface: 800 RU
Bmax: 735 RU
Kd: 144 nM
NGL2 binding NetrinG1 (swapped loop I+II+III)
Surface: 800 RU
Bmax: 670 RU
Kd: 12 µM
NGL1 binding NetrinG2 (swapped loop I+II+III)
Surface: 590 RU
Bmax: 436 RU
Kd: 6.7 µM
NGL2 binding NetrinG2 (swapped loop I+II+III)
Surface: 590 RU
Bmax: N/A
Kd: N/A
NetrinG1 binding to NGL1 (A205T*)
Surface: 380 RU
Bmax: N/A
Kd: N/A
NetrinG2 binding to NGL1 (A205T*)
Surface: 680 RU
Bmax: N/A
Kd: N/A
NetrinG1 binding to NGL2 (G204T*)
Surface: 500 RU
Bmax: N/A
Kd: N/A
NetrinG2 binding to NGL2(G204T*)
Surface: 500 RU
Bmax: N/A
Kd: N/A
NetrinG1 binding NGL1-r123
Surface: 750 RU
Bmax: N/A
Kd: N/A
NetrinG2 binding NGL1-r123
Surface: 750 RU
Bmax: 497 RU
Kd: 26 nM
NetrinG1 binding NGL2-r123
Surface: 350 RU
Bmax: 193 RU
Kd: 160 nM
NetrinG2 binding NGL2-r123
Surface: 350 RU
Bmax: 172 RU
Kd: 6 µM
NetrinG1 binding NGL1-r1
Surface: 650 RU
Bmax: 469 RU
Kd: 118 nM
NetrinG2 binding NGL1-r1
Surface: 650 RU
Bmax: 307 RU
Kd: 1.6 µM
NetrinG1 binding NGL1-r2
Surface: 800 RU
Bmax: 545 RU
Kd: 44 nM
NetrinG2 binding NGL1-r2
Surface: 800 RU
Bmax: 511 RU
Kd: 12.3 nM
NetrinG1 binding NGL1-r3
Surface: 780 RU
Bmax: 433 RU
Kd: 810 nM
NetrinG2 binding NGL1-r3
Surface: 780 RU
Bmax: 378 RU
Kd: 134 nM
NetrinG1 binding to NGL3
Surface: 860 RU
Bmax: 569 RU
Kd: 167 µM#
NetrinG2 binding to NGL3
Surface: 860 RU
Bmax: 512 RU
Kd: 141 µM#
Response (RU)
Concentration (M)

Supplementary figure 8. NGL-NetrinG interaction specificity depends on distinctive binding surfaces. (A) Affinities of NGL1 (blue) and NGL2 (red) binding to immobilized NetrinG constructs were normalized using the K_d value measured for intra-class binding to the corresponding wild type NetrinG (WT). Affinities that were too low to measure using the chosen method are indicated by an asterisk (blue or red). We created NetrinG knock out mutants (KO) by introducing an N-linked glycosylation site in loop I designed to block the interaction (NetrinG1 P85A+Y86T, NetrinG2 P74A+Y75T, NGL1 A205T, NGL2 G204T). To test the contribution of NetrinG loops I-III on NetrinG-NGL binding specificity, we transplanted individual loops from NetrinG1 into NetrinG2, and, *vice versa*, exchanged individual NetrinG1 loops with the equivalent sequence found in NetrinG2. The data reveal that swapping loop I decreases the affinity for intra-class and cross-class binding, thereby suggesting that loop I depends on its native protein context for efficient binding to NGL. Intriguingly, swapping NetrinG1 loop II to that of NetrinG2 leads to a small increase of affinity to NGL1, and loss of affinity to NGL2. The reverse swap in NetrinG2 also increases NGL1-binding and reduces the affinity to NGL2, overall equalizing the affinity to the two NGLs. Swapping NetrinG1 loop III to that of NetrinG2 leads to an increase (~10-fold) in affinity to both NGL1 and NGL2, while the reverse swap in NetrinG2 abolishes binding to either. Taken together, these results imply that the extra interactions provided by NetrinG2 loop III are beneficial for binding either NGL receptor, regardless of the NetrinG context. Swapping NetrinG2 loop III in combination with loop II, or all three loops at once, creates proteins that still binds weakly to NGL1, but not to NGL2, and thus has a switched binding preference compared to the native protein. However, the corresponding NetrinG1 mutants did not result in switched specificity. Overall, the data suggest that NetrinG loops do not function as stand-alone elements and that transplanting them into a non-native protein context can affect their NGL-binding properties. (B) Fitted SPR data (1:1 Langmuir binding model) are presented for all mutant $NGL_{LRR\text{-}Ig}$ and $NetrinG_{Lam\text{-}EGF}$ constructs. Black asterisks mark mutations that lead to the introduction of an N-linked glycosylation site within the NetrinG-NGL binding interface (=KO mutants). A hash (#) marks K_d values that were too low to determine accurately using this method.

REFERENCES

Aricescu AR, Lu W, Jones EY (2006) A time- and cost-efficient system for high-level protein production in mammalian cells. *Acta Crystallogr D Biol Crystallogr* **62:** 1243-1250

Chang VT, Crispin M, Aricescu AR, Harvey DJ, Nettleship JE, Fennelly JA, Yu C, Boles KS, Evans EJ, Stuart DI, Dwek RA, Jones EY, Owens RJ, Davis SJ (2007) Glycoprotein structural genomics: solving the glycosylation problem. *Structure* **15:** 267-273

Felsenstein J. (1993) PHYLIP (Phylogeny Inference Package) version 3.5c.

Gupta R, Jung E, Brunak S (2004, in preparation) Prediction of N-glycosylation sites in human proteins.

Hussain SA, Carafoli F, Hohenester E (2011) Determinants of laminin polymerization revealed by the structure of the alpha5 chain amino-terminal region. *EMBO Rep* **11:** 11

Kwon SK, Woo J, Kim SY, Kim H, Kim E (2010) Trans-synaptic adhesions between netrin-G ligand-3 (NGL-3) and receptor tyrosine phosphatases LAR, protein-tyrosine phosphatase delta (PTPdelta), and PTPsigma via specific domains regulate excitatory synapse formation. *J Biol Chem* **285:** 13966-13978.

Lin JC, Ho WH, Gurney A, Rosenthal A (2003) The netrin-G1 ligand NGL-1 promotes the outgrowth of thalamocortical axons. *Nat Neurosci* **6:** 1270-1276.

Mosyak L, Wood A, Dwyer B, Buddha M, Johnson M, Aulabaugh A, Zhong X, Presman E, Benard S, Kelleher K, Wilhelm J, Stahl ML, Kriz R, Gao Y, Cao Z, Ling HP, Pangalos MN, Walsh FS, Somers WS (2006) The structure of the Lingo-1 ectodomain, a module implicated in central nervous system repair inhibition. *J Biol Chem* **281:** 36378-36390.

Nishimura-Akiyoshi S, Niimi K, Nakashiba T, Itohara S (2007) Axonal netrin-Gs transneuronally determine lamina-specific subdendritic segments. *Proc Natl Acad Sci U S A* **104:** 14801-14806.

Ramelot TA, Raman S, Kuzin AP, Xiao R, Ma LC, Acton TB, Hunt JF, Montelione GT, Baker D, Kennedy MA (2009) Improving NMR protein structure quality by Rosetta refinement: a molecular replacement study. *Proteins* **75:** 147-167.

Zhang W, Rajan I, Savelieva KV, Wang CY, Vogel P, Kelly M, Xu N, Hasson B, Jarman W, Lanthorn TH (2008) Netrin-G2 and netrin-G2 ligand are both required for normal auditory responsiveness. *Genes Brain Behav* **7:** 385-392.